Naturally Occurring Asbestos: Potential for Human Exposure, Southern Nevada, USA

Brenda J. Buck*
Dep. of Geoscience
Univ. of Nevada-Las Vegas
4505 S. Maryland Pkwy.
Las Vegas, NV 89154-4010

Dirk Goossens
Dep. of Geoscience
4505 S. Maryland Pkwy.
Univ. of Nevada-Las Vegas
Las Vegas, NV 89154-4010
and
Geography Research Group
Dep. of Earth and Environmental Sciences
Geo-Institute
KU Leuven
Celestijnenlaan 200E
3001 Leuven, Belgium

Rodney V. Metcalf
Dep. of Geoscience
4505 S. Maryland Pkwy.
Univ. of Nevada-Las Vegas
Las Vegas, NV 89154-4010

Brett McLaurin
Dep. of Environmental, Geographical and Geological Sciences
Bloomsburg Univ. of Pennsylvania
400 E. Second St.
Bloomsburg, PA 17815

Minghua Ren
Frederick Freudenberger
Dep. of Geoscience
4505 S. Maryland Pkwy.
Univ. of Nevada-Las Vegas
Las Vegas, NV 89154-4010

Amphibole asbestos minerals are known human carcinogens, and many regulations have been developed to limit occupational exposure. These minerals can also occur in the natural environment, where they may be more difficult to control. We applied a diverse set of analytical methods including scanning electron microscopy/energy dispersive spectroscopy, electron probe analysis, x-ray diffraction, and field-emission scanning electron microscopy to rock, soil, and dust samples and to particles attached to clothing samples and cars. We found naturally occurring fibrous actinolite, a regulated amphibole asbestos mineral, in rock, soil, and dust that can be transported by wind, water, cars, or on clothing after outdoor recreational activities. Sources of these fibrous amphiboles are several plutons in southern Nevada and Arizona and alluvial fans emanating from asbestos-containing bedrock. The morphology of the amphibole fibers is similar to amphibole fibers found in the USEPA Superfund site at Libby, MT. We found that the morphometry of the fibrous particles in the study area did not substantially change when the original bedrock weathered into soil, and particles were eroded and transported through wind and/or water and finally settled and accumulated on natural or other surfaces. Because large populations in Boulder City, Henderson, and Las Vegas are located only a few kilometers, sometimes even only a few tens of meters, downwind from the sources, and because most of the particles are transported in suspension after they are emitted, potentially large populations in Boulder City, Henderson, and perhaps Las Vegas could be exposed. This study demonstrates a potential public health risk to several large population areas.

Abbreviations: EDS, energy dispersive spectroscopy; FE-SEM, field-emission scanning electron microscopy; IMA, International Mineralogical Association; SEM, scanning electron microscopy; XRD, x-ray diffraction.

Amphibole asbestos minerals (riebeckite, grunerite-cummingtonite, anthophyllite, tremolite, actinolite) are known human carcinogens (Agency for Toxic Substances and Disease Registry, 2001; International Agency for Research on Cancer, 2012). Exposure to fibrous amphiboles can cause asbestosis; lung, ovarian, and larynx cancer; mesothelioma; pleural fibrosis; and possibly other health effects including depressed immune function, cardiovascular disease, and gastrointestinal cancer (Agency for Toxic Substances and Disease Registry, 2001; Camargo et al., 2011; International Agency for Research on Cancer, 2012; Shannahan et al., 2012).

Although amphibole minerals are common, fibrous and asbestiform amphiboles are less so and require specific geologic processes that promote the growth of fibers, in particular rock deformation during or subsequent to amphibole growth (Ahn and Buseck, 1991; Virta, 2002). The complexity of amphibole fiber formation is reflected in their widely varying chemical composition, which

Soil Sci. Soc. Am. J. 77:2192–2204
doi:10.2136/sssaj2013.05.0183
Open Access Article
Received 16 May 2013.
*Corresponding author (buckb@unlv.nevada.edu).
© Soil Science Society of America, 5585 Guilford Rd., Madison WI 53711 USA
All rights reserved. No part of this periodical may be reproduced or transmitted in any form or by any means, electronic or mechanical, including photocopying, recording, or any information storage and retrieval system, without permission in writing from the publisher. Permission for printing and for reprinting the material contained herein has been obtained by the publisher.

determines their mineralogical classification (Leake et al., 1997; Hawthorne et al., 2012). Many amphibole minerals form solid solution series, which are variations in chemical composition among two or more end members. Mineral names, therefore, represent a range of chemical composition, and specific mineral names cannot be accurately assigned without chemical analysis using an electron microprobe (Meeker et al., 2003). Additionally, amphibole asbestos classification has been complicated by the use of industrial names (Lowers and Meeker, 2002; Meeker et al., 2003): for example, crocidolite and blue asbestos for riebeckite, and amosite for cummingtonite-grunerite (Virta, 2002). Complications also arise because of evolving amphibole classification schemes used by mineralogists (Leake, 1978; Leake et al., 1997; Hawthorne et al., 2012).

Further complications arise from the use of terms to describe the crystal morphology of fibrous amphiboles (Lowers and Meeker, 2002), in particular the term *asbestiform* as applied to the regulation of commercial asbestos (Meeker, 2009). The definition of asbestiform for regulatory purposes generally sets limits on size (diameter <0.5 μm) and aspect ratio (>20:1), with additional morphological characteristics (Lowers and Meeker, 2002). It has long been known, however, that inhaling such minerals when they occur as long, thin fibers can cause disease, including those minerals that can be described as fibrous but fall outside the narrower definition of asbestiform (Agency for Toxic Substances and Disease Registry, 2001; Camargo et al., 2011; Meeker, 2009; International Agency for Research on Cancer, 2012). *Naturally occurring asbestos* refers to asbestos found as a natural component of rocks and soils but may include fibrous minerals that do not meet the regulatory definition of asbestos (Harper, 2008).

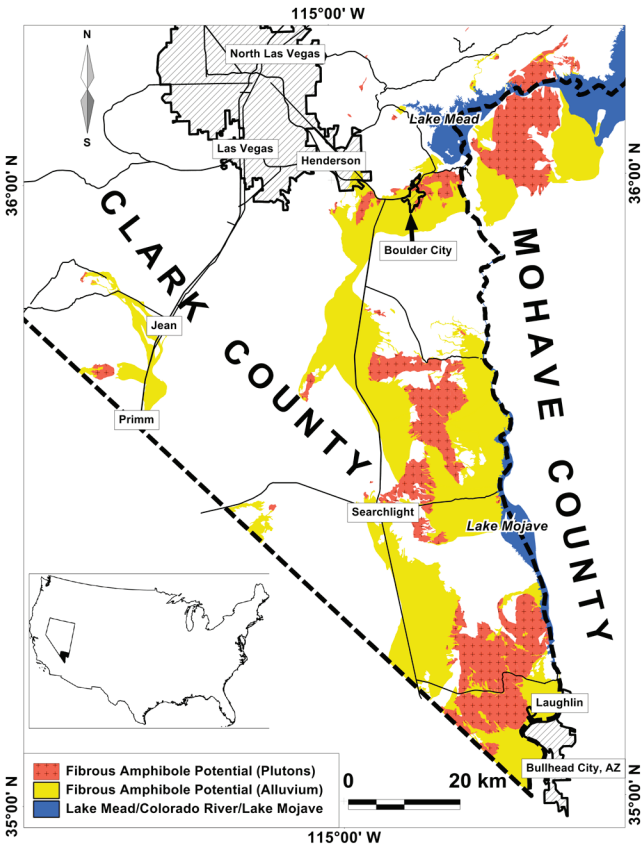

Fig. 1. Predicted potential occurrences of fibrous amphiboles in Clark County, Nevada, and an area of adjacent Mohave County, Arizona, south of western Lake Mead. Plutons are Miocene in age; alluvium includes deposits of Miocene to Quaternary age. Only a small portion of these mapped areas has been examined.

In addition to the regulated asbestos minerals, many other naturally occurring fibrous minerals are also implicated in causing disease. Examples include the amphibole minerals winchite, magnesioriebeckite, and richterite from studies in Libby, MT (e.g., Meeker et al., 2003; Shannahan et al., 2012), erionite (a zeolite mineral) in Turkey and North Dakota (Carbone et al., 2011; Ryan et al., 2011), and antigorite (a serpentine mineral) in Poland (Wozniak et al., 1988) and New Caledonia (Baumann et al., 2010). Toxicity is related to the width, length, aspect ratio, surface area, and surface chemical composition of the mineral fiber (Aust et al., 2011). Separable fibers longer than 5 μm with aspect ratios ≥3:1 and those that contain Fe are considered to be more toxic (Aust et al., 2011; Case et al., 2011). Morphology, along with amphibole classification, is at the heart of controversies over the potential public health risks and the necessity for remediation represented by naturally occurring asbestos. An example includes the naturally occurring fibrous actinolite-magnesiohornblende in the northern California community of El Dorado Hills (Harper, 2008; Meeker et al., 2006). Additionally, during the Libby, MT, criminal trial, defense experts for the mining company argued on the basis of morphology and amphibole classification that the Libby amphiboles fell outside the regulatory definition of asbestos (Meeker, 2009), despite clear evidence for high rates of asbestos-related disease in the Libby population (Agency for Toxic Substances and Disease Registry, 2002).

Previous to this study, there were no reported natural occurrences of asbestos in Clark County, Nevada (Van Gosen, 2008). Fibrous blue amphiboles (magnesioriebeckite, winchite, and actinolite) similar to those at Libby, MT, have been reported from Miocene granitoid plutons (igneous intrusions) in an area of Mohave County, Arizona (Fig. 1), immediately adjacent to Clark County, Nevada (Potts and Metcalf, 1997; Potts, 2000). These fibrous amphiboles were formed by hydrothermal alteration of faulted Miocene plutonic rock and are present as fracture-fill veins and replacement of primary magmatic amphibole (Potts and Metcalf, 1997; Potts, 2000). Subsequent erosion of the altered pluton redistributed clasts containing fibrous amphibole into Miocene conglomerates (Williams, 2003) as well as more recent Quaternary alluvium. The fibrous amphibole occurrences in Mohave County are all within unpopulated areas of the Lake Mead National Recreation Area; however, similar faulted and altered Miocene plutonic rocks and related conglomerate–alluvium deposits crop out in and near populated areas of Clark County (Fig. 1). Therefore, in this study, we initiated an exploration for fibrous amphiboles using existing geologic maps and our expertise to create a map showing areas that contain the types of rocks that could potentially contain known or suspected carcinogenic fibrous amphiboles (Fig. 1). Field exploration of

one of these areas in the McCullough Range south of Las Vegas found fibrous blue and green amphibole minerals lining fractures within Miocene granitoid plutons. Based on these results, we decided to perform an initial exploration of this immediate area and its surroundings and determine the presence, location, mineralogy, and morphology of the fibrous amphiboles in rock, soil, and dust to guide future research on the potential human health risk.

MATERIALS AND METHODS

Forty-three samples were collected (Table 1). Seventeen rock samples were collected from exposed granitoid outcrops: seven from Boulder City, four from Black Hill, and six from the McCullough Range (Fig. 2). Rock samples were collected by using a rock hammer to break fresh samples from exposed outcrops. Seventeen soil samples were collected, among which 11 were from pristine desert surfaces and six from dirt roads (Fig. 2). Soil was collected using a plastic scoop and sampling the uppermost <1-cm loose soil from the surface. Airborne sediment was collected using Big Spring Number Eight (BSNE) dust traps (Fryrear, 1986) set at four levels: 25, 50, 75, and 100 cm. Dust collected at heights of 25 and 100 cm was analyzed for fibrous amphiboles using scanning electron microscopy (SEM) with an attached energy dispersive spectroscopy (EDS) detector (see below). One trap was placed in the backyard of a private residence in Boulder City from 3 to 18 Nov. 2012. This private residence was chosen because the backyard was exposed to the undeveloped, open desert. Other traps were placed downwind adjacent to dirt roads while vehicles (cars, trucks, and/or motorcycles) traversed them for a period of a few hours. Lastly, four samples were collected from clothing (pants and boots) and the side of a car tire after a single morning of outdoor recreation in Boulder City. Activities during this time included driving and walking on dirt roads. The clothes and the car were washed before and sampled after the recreation activities.

Samples were analyzed at the University of Nevada-Las Vegas using a variety of analytical methods (see Table 1) including: (i) SEM/EDS, (ii) field-emission scanning electron microscopy (FE-SEM), (iii) x-ray diffraction (XRD) analysis, and (iv) wavelength dispersive electron probe microanalysis (EPMA). For initial SEM/EDS and FE-SEM analyses, green and blue minerals visually identified as amphiboles in rock samples were mounted on aluminum stubs with carbon tape. Dust and soil samples were mounted by pressing aluminum stubs with carbon tape against the sides of the plastic bags (e.g., Meeker et al., 2003). Later, to more accurately measure particle size and shape, all soil samples, two partially disintegrated rock samples (Adams2 and H8R), and most BSNE dust samples were sieved through a 250-μm sieve. A total of 0.2 g was then put into 40 mL of deionized water and stirred with a magnetic stirring device. A 100-μL aliquot of each sample was collected and placed on a separate 0.4-μm pore diameter polycarbonate filter (see

Table 1. Sample locations, type, and analyses performed using scanning electron microscopy (SEM), energy dispersive spectroscopy (EDS), field-emission scanning electron microscopy (FE-SEM), x-ray diffraction (XRD), and/or wavelength dispersive electron probe microanalysis (EPMA).

Sample	GPS coordinates†		Sample type	Analyses performed		
	Easting	Northing		SEM/EDS/FESEM	XRD	EPMA
B3	696807	3982012	soil (road)	x		
B4	697117	3983568	soil (road)	x		
B6	696008	3981309	soil (road)	x		
B8	695904	3981177	soil (road)	x		
H6	685692	3982619	soil (road)	x		
H7	685229	3982251	soil (road)	x		
B1	696156	3978305	soil	x		
B2	696566	3980472	soil	x		
B7	695969	3981257	soil	x		
H3	686668	3983593	soil	x		
H4	686541	3983520	soil	x		
H5	686052	3983145	soil	x		
B10	688020	3978798	soil	x		
B11	686454	3973088	soil	x		
B9	688767	3981258	soil	x		
H8	682517	3980875	soil	x		
H9	682214	3981162	soil	x	x	
Adams	694756	3982651	rock	x	x	
Adams2	694756	3982651	rock	x		x
Adams3	694756	3982651	rock	x		
BCP1	696326	3982163	rock	x		
BCP2	696326	3982163	rock	x		
BCP3	696326	3982163	rock	x	x	
BCP4	696326	3982163	rock	x		x
F1	685884	3981679	rock	x		
F1.5	685884	3981679	rock	x		
F2	685884	3981677	rock	x		
H8R	686052	3983145	rock	x		
MR2A	682216	3981145	rock	x		
MR2B	682216	3981145	rock	x		x
RJ1	682216	3981145	rock	x	x	
RBKT1	682610	3982218	rock	x		
RBKT2	682610	3982218	rock	x		
RBKT3	683989	3978374	rock	x		
BCF	696326	3982163	dust	x		
D1	696979	3983107	dust	x		
D4	696979	3983107	dust	x		
H8D	682517	3980875	dust	x		
H9D	682214	3981162	dust	x		
P	‡		dust (pants)	x		
LR	‡		dust (boots)	x		
LL	‡		dust (boots)	x		
C	‡		dust (car tire)	x		

† GPS coordinates are referenced to NAD 83 UTM Zone 11 North.

‡ Collected from dust after recreational activities in Boulder City.

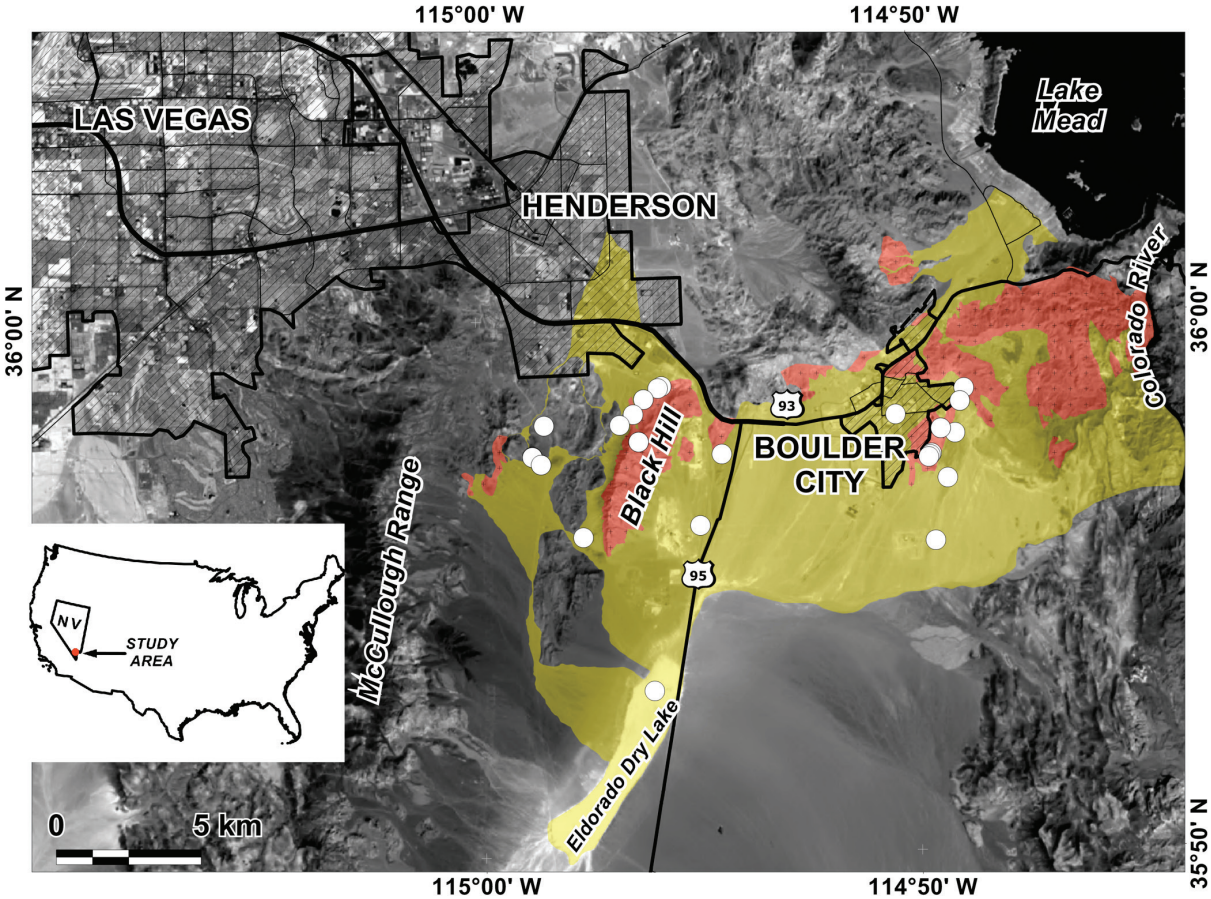

Fig. 2. Landsat image showing the study area in southern Nevada. Granitic plutons are shown in red. Estimated areas of alluvium deposited from erosion of those plutons are shown in yellow. All sampling locations are shown as white circles and contained fibrous amphiboles.

Meeker et al., 2006). For two BSNE samples (BCF and H9D), most rock samples, and the dust samples from clothing and the car tire, the quantities of loose sediment were too small to collect 0.2 g of sediment and the initial method was used.

Stubs and filters were coated with C and analyzed using a JEOL SEM (JSM5600) equipped with an Oxford EDS detector and/or a FE-SEM (JSM6700F) (Table 1). Samples were scanned for amphibole fibers at magnifications ranging from 500 to 2000×. Particle dimensions were measured through a combination of using the JEOL PC-SEM software calibrated with a certified JEOL mag-standard (for FE-SEM images) and individually measuring SEM images using the scales provided with each image. Aspect ratios were calculated using the maximum length and average width of each particle as was done in previous studies (Campbell et al., 1977; Meeker et al., 2003, 2006) and to make accurate calculations of particle volume necessary to calculate the terminal fall velocity (see below).

A PANalytical X'Pert Pro x-ray diffraction spectrometer was used to analyze three rock samples and one soil sample. The samples were ground to a fine powder with a mortar and pestle and analyzed at the following settings: 20 mA at 40 kV, °2θ values 5 to 75; data were analyzed using X'Pert Pro software.

Amphibole mineralogical classification was based on quantitative chemical analyses of three polished thin-sections measured on a four-wavelength dispersive spectrometer, automated JEOL 8900 electron probe microanalyzer. Amphibole structural formulae calculations were performed using the EPMA data following recommendations of the International Mineralogical Association (IMA) (Leake et al., 1997); amphibole names were evaluated using both the Leake et al. (1997) and Hawthorne et al. (2012) IMA classification schemes. The fibrous nature of the amphiboles can result in poor polishing in probe sections, which in turn can result in lower oxide totals in electron probe microanalyses than might normally be expected (Meeker et al., 2006). Following the approach used by the USGS EPMA laboratory in Denver (Meeker et al., 2006), we rejected any analyses that yielded totals <92% (w/w).

The atmospheric transport mode was determined for 765 confirmed amphibole particles. The atmospheric transport mode of a particle can be derived from the ratio u_∞/u_*, where u_∞ is the terminal fall velocity of the particle and u_* is the friction velocity (Pye and Tsoar, 1990). The following transport modes apply: saltation ($u_\infty/u_* > 1.25$): particle transport on the order of centimeters to a few meters, up to a few tens of meters when particles experience succeeding jumps in a windstorm; modified saltation ($0.70 < u_\infty/u_* < 1.25$): particle transport from a few meters to a few hundreds of meters; short-term suspension ($0.10 < u_\infty/u_* < 0.70$): particle transport from a few hundreds of meters to several tens of kilometers; and long-term suspension ($u_\infty/u_* < 0.10$): particle transport up to hundreds of kilometers and more. For nonspherical particles such as fibers,

which tend to have a cylindrical shape, u_∞ can be calculated with the formula of Dietrich (1982), taking the volume equivalent diameter as the reference particle diameter and setting the Powers Index (Folk, 1965) equal to 6. Dietrich's formula was derived for particle Reynolds numbers (Re) larger than approximately 0.1. Comparisons with experimental data sets (Goossens, 1987a) have shown that Dietrich's formula provides excellent results for Corey shape factors (Corey, 1949) >0.20. For Corey shape factors <0.20 and Re >1.0, the formula of Vakil and Green (2009) can be used. For Corey shape factors <0.20 and Re <1.0, the formula

$$u_\infty = \frac{\left(\rho_p - \rho_f\right)\pi g \sqrt[3]{6L^4R^5}}{12\eta_f\left(R\pi\sin\alpha + 2L\cos\alpha\right)}$$

(see Appendix A) can be used, where ρ_p is the mass density of the particle, ρ_f is the mass density of air, g is gravitational acceleration, L is the length of the particle, R is the radius of the particle, η_f is the dynamic viscosity of air, and α is the inclination of the particle in the flow ($\alpha = 90°$ for orientation parallel to the flow and $\alpha = 0°$ for orientation perpendicular to the flow). For Re <0.1 (laminar flow), the orientation of particles is random ($\alpha = 45°$), whereas for Re >1 (turbulent flow), particles tend to orient themselves perpendicular to the flow ($\alpha = 0°$) (Goossens, 1987b). For the interval 0.1 < Re < 1.0, the flow is transitional. Calculations for the fibers investigated in this study showed that, in the transitional regime, $\alpha = 45°$ leads to much better agreement with Dietrich's formula than $\alpha = 0°$, suggesting that particles are still more or less randomly oriented. Therefore, for Re <1.0, a value of 45° was used when calculating u_∞.

Geospatial methods used data from existing geologic maps, data sets, and GIS software. A map for initial exploration was created using data from House et al. (2010) and Felger and Beard (2010) to delineate areas in Clark County and northwestern Arizona that could potentially contain fibrous amphiboles (Fig. 1). On the House et al. (2010) map, these include Miocene granitoid plutons and large alluvial deposits eroded from them. The estimated areas draining plutonic rocks in Fig. 2 were created within a GIS database by digitizing and integrating topography, hydrology, and aerial photography data sets (National Elevation Dataset, http://ned.usgs.gov; National Hydrology Dataset, http://nhd.usgs.gov; and the Geospatial Data Gateway, http://datagateway.nrcs.usda.gov). These data were superimposed on the geologic data compiled from House et al. (2010), Anderson (1977), and Smith (1984) to determine the intersection of these drainages with exposed granitic plutons in the study area.

RESULTS

Occurrence

All 43 samples, including rock, soil, dust, car tire, and clothing, contained fibrous amphiboles. The original sources of these fibrous amphiboles are the Miocene plutons in the McCullough Range, Black Hill, and Boulder City areas (Fig. 2). Fibrous amphiboles in these granitoid plutons occur as fracture-fill veins and as alteration products of primary magmatic amphibole and appear hydrothermal in origin. In the McCullough Range and Black Hill, sediment eroded from these sources forms large alluvial fans that drain primarily eastward into the Eldorado Dry Lake, along the western side of Highway 95, and north–northwest along the southeastern edge of the city of Henderson. In Boulder City, sediment eroded from the pluton is deposited in many areas in and surrounding the city (Fig. 2).

If we assume that our samples are representative of the surrounding geomorphic surfaces, the estimated total surface area either containing fibrous amphiboles or likely to contain them (plutons plus alluvial fans in Fig. 2) is approximately 214 km^2, which corresponds to about 53,000 acres. This calculation does not include the fibrous amphibole locality in Mohave County, Arizona (Potts, 2000; Williams, 2003), just east of the Colorado River (Fig. 1; center right of Fig. 2). Additionally, other Miocene plutons in the region have not yet been studied but may also have the potential to contain similar fibers (Fig. 1). Thus, the precise locations and full extent of fibrous amphiboles in this region remains to be determined.

Mineralogy

Although XRD analyses cannot identify specific amphibole phases (Meeker et al., 2003), our analyses indicate the presence of amphibole: whole rock and soil samples analyzed by XRD identified albite, amphibole, quartz, calcite, chlorite, and biotite. Electron microprobe analysis of fibrous amphiboles (111 analyses) in rocks from Boulder City and the McCullough Range identified these amphiboles primarily as actinolite (85%), one of the six regulated asbestos minerals (Fig. 3; Table 2). Some analyses from Sample MR2B were classified as magnesiohornblende; these analyses are clearly part of a solid solution compositional continuum with actinolite in the same sample (Fig. 3; Table 2). We

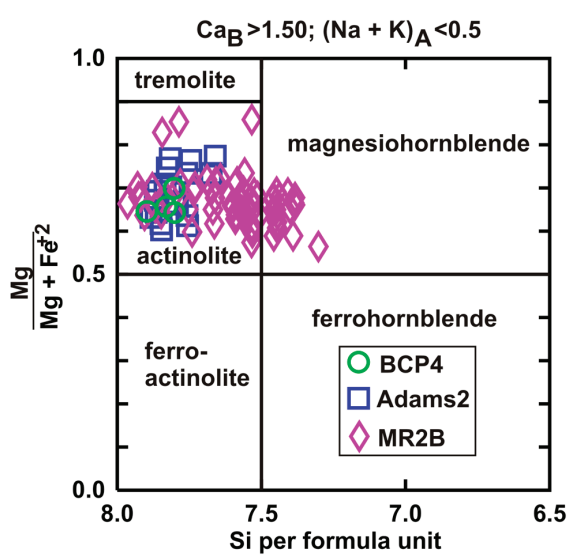

Fig. 3. Mineralogy of fibrous amphiboles in southern Nevada. Structural formula calculations, including Fe^{3+} estimates, and amphibole classifications follow the 1997 recommendations of the International Mineralogical Association (Leake et al., 1997). Most analyses classified as actinolite, which is one of six regulated asbestos minerals. Sites BCP4 and Adams2 are from the Boulder City pluton; MR2B is from the McCullough Range near Henderson.

are not aware of reports of asbestiform magnesiohornblende in the literature, but actinolite-magnesiohornblende at El Dorado Hills, CA, is described as having "fibrous to prismatic" morphology (Meeker et al. 2006, p. 20). The 1997 IMA classification scheme (Leake et al., 1997) was used in Fig. 3 to facilitate comparison with prior work on fibrous amphiboles (e.g., Meeker et al., 2006). Using the more recent IMA 2012 classification (Hawthorne et al., 2012), the majority of our analyses (98%) were classified as actinolite (most analyses that classified as magnesiohornblende using IMA 1997 were reclassified as actinolite using IMA 2012).

Table 2. Mineral chemistry data for analyses of 16 selected points from three representative samples. Results for other analyses were similar. Oxide concentrations from wavelength dispersive electron probe microanalysis; structural formula calculations according to Leake et al. (1997).

Sample ID	BCP4				Adams2						MR2B					
Point	rim1	rim4	rim5	am5-13	am1-18	am2-4	am2-24	am3-9	am3-11	am3-14	rim1-7	am1-4	vein1-2	vein1-4	vein1-14	am3-12
Mineralogy†	Act	Act	Act	Act	Act	Act	Act	Act	Act	Act	Act	Act	Mg-hbld	Act	Act	Act
								Oxides, % (w/w)								
SiO_2	53.79	54.02	52.07	54.12	54.32	52.37	53.27	53.90	54.22	53.95	54.41	53.18	51.03	51.22	51.84	50.68
Al_2O_3	1.12	1.52	1.62	1.31	1.62	1.48	1.55	1.40	1.19	1.81	0.68	2.33	3.86	2.97	4.05	4.46
TiO_2	0.03	0.03	0.02	0.10	0.10	0.17	0.18	0.13	0.11	0.12	0.06	0.18	0.18	0.13	0.10	0.14
MnO	0.60	0.61	0.55	0.54	0.20	0.26	0.24	0.74	0.44	0.22	0.30	0.30	0.26	0.30	0.25	0.27
MgO	14.27	14.61	13.71	15.50	17.09	13.64	14.12	16.06	13.40	15.93	14.95	16.02	13.40	13.61	14.42	14.09
FeO‡	14.17	13.90	14.01	13.10	11.14	16.02	15.59	14.26	16.76	11.82	14.15	11.82	15.83	15.40	12.64	14.32
CaO	12.18	12.66	12.52	12.53	12.82	12.03	12.10	9.43	12.07	11.99	11.04	12.49	12.54	12.60	12.34	12.70
Na_2O	0.28	0.25	0.22	0.32	0.23	0.55	0.58	0.37	0.47	0.30	1.07	0.58	0.63	0.60	0.84	0.76
K_2O	0.06	0.09	0.11	0.09	0.07	0.09	0.09	0.06	0.09	0.11	0.07	0.16	0.19	0.18	0.15	0.15
F	0.00	0.00	0.14	0.16	0.09	0.00	0.00	0.00	0.00	0.00	0.23	0.23	0.00	0.00	0.22	0.07
Cl	0.04	0.02	0.05	0.00	0.01	0.01	0.01	0.09	0.02	0.08	0.04	0.14	0.08	0.13	0.07	0.07
Total	96.56	97.71	94.96	97.73	97.67	96.67	97.75	96.41	98.77	96.35	96.93	97.33	97.99	97.12	96.82	97.67
								Calculated structural formula per 23 oxygens								
T site§																
Si	7.897	7.830	7.801	7.803	7.745	7.756	7.758	7.868	7.846	7.834	7.918	7.688	7.452	7.549	7.574	7.386
Al(T)	0.103	0.170	0.199	0.197	0.255	0.244	0.242	0.132	0.154	0.166	0.082	0.312	0.548	0.451	0.426	0.614
Sum	8.000	8.000	8.000	8.000	8.000	8.000	8.000	8.000	8.000	8.000	8.000	8.000	8.000	8.000	8.000	8.000
C site§																
Al(C)	0.090	0.090	0.086	0.025	0.017	0.014	0.025	0.109	0.050	0.144	0.033	0.085	0.117	0.065	0.272	0.151
Ti	0.003	0.003	0.003	0.011	0.011	0.019	0.020	0.014	0.012	0.013	0.007	0.020	0.020	0.014	0.011	0.016
Fe^{3+}	0.025	0.034	0.055	0.146	0.204	0.078	0.143	0.029	0.121	0.020	0.192	0.080	0.219	0.164	0.001	0.206
Mg	3.124	3.157	3.062	3.332	3.631	3.011	3.067	3.495	2.891	3.449	3.244	3.451	2.916	2.990	3.142	3.062
Fe^{2+}	1.683	1.641	1.700	1.421	1.114	1.845	1.716	1.262	1.873	1.347	1.486	1.326	1.696	1.729	1.542	1.532
Mn	0.075	0.075	0.070	0.066	0.024	0.033	0.030	0.091	0.053	0.027	0.037	0.037	0.033	0.038	0.031	0.033
Sum	5.000	5.000	4.976	5.000	5.000	5.000	5.000	5.000	5.000	5.000	5.000	5.000	5.000	5.000	5.000	5.000
B site§																
Mn	0.031	0.010	0.000	0.012	0.010	0.033	0.030	0.091	0.034	0.027	0.037	0.023	0.018	0.005	0.000	0.008
Fe^{2+}	0.031	0.010	0.000	0.012	0.000	0.027	0.010	0.359	0.000	0.042	0.007	0.000	0.000	0.000	0.000	0.000
Ca	1.915	1.966	2.009	1.936	1.959	1.909	1.888	1.475	1.871	1.866	1.721	1.935	1.961	1.990	1.931	1.983
Na	0.054	0.025	0.000	0.051	0.031	0.031	0.072	0.076	0.095	0.066	0.236	0.042	0.021	0.006	0.068	0.009
Sum	2.000	2.000	2.009	2.000	2.000	2.000	2.000	2.000	2.000	2.000	2.000	2.000	2.000	2.000	2.000	2.000
A site§																
Na	0.024	0.047	0.065	0.039	0.032	0.127	0.091	0.029	0.037	0.019	0.065	0.119	0.158	0.165	0.170	0.206
K	0.012	0.017	0.020	0.017	0.013	0.018	0.016	0.012	0.016	0.021	0.014	0.030	0.036	0.034	0.028	0.029
Sum	0.036	0.063	0.085	0.056	0.045	0.145	0.107	0.041	0.054	0.040	0.079	0.149	0.193	0.199	0.198	0.234
Total cations	15.04	15.06	15.07	15.056	15.045	15.145	15.107	15.041	15.054	15.04	15.079	15.149	15.193	15.199	15.198	15.234
Mg¶	0.65	0.66	0.64	0.70	0.76	0.61	0.64	0.67	0.60	0.71	0.68	0.72	0.63	0.63	0.67	0.67
Avg. Fe^{3+}, %	0.01	0.02	0.03	0.09	0.15	0.04	0.08	0.02	0.06	0.01	0.11	0.06	0.11	0.09	0.00	0.12

† Act, actinolite; Mg-hbld, magnesiohornblende.

‡ Total Fe.

§ T, C, B, and A sites refer to specific cation sites in the amphibole structural formula $A_{0\text{-}1}C_2B_5T_8O_{22}(OH_2)$; Al(T) and Al(C) are the Al that is calculated to occur in the T and C sites, respectively.

¶ $Mg/(Mg + Fe^{2+})$.

Morphology

The Nevada amphibole particles occur in many different morphologies ranging from blocky crystals to flexible fiber bundles and individual fibers (Fig. 4 and 5). The nomenclature used to describe the mineral habit is not consistent and can be problematic (Meeker et al., 2003, 2006). Often, morphological definitions cannot be determined through SEM analyses, and most importantly, morphological definitions may not provide an accurate assessment of actual health risks (Meeker et al., 2003, 2006). Because fiber morphology is part of regulatory definitions (Crane, 1995), however, morphologic differentiation is an important issue. In this study, individual fibers were defined as individual, narrow, usually very elongated crystals with straight, even edges (Fig. 4a and 5c). They may contain visual fibrils. Fiber bundles were defined as elongated amphiboles showing evidence of being in the process of separating into smaller fibers (Fig. 4b–4e). Many fibers and fiber bundles often showed evidence of curling or bending (Fig. 4b, 4c, 5d, and 5e). Some bundles and curved fibers fit the definition of asbestiform (Lowers and Meeker, 2002). We classified prismatic crystals as any amphibole crystal that occurred with irregular, blunt edges and did not have fibers peeling away from the larger mass (Fig. 4f). Some of the latter may be cleavage fragments; however, since it is not possible with individual crystals to know if they have broken away from a larger crystal (Meeker et al., 2006), we cannot distinguish between prismatic crystals and cleavage fragments. When not defining specific morphologies, we use the generic term *particle* here.

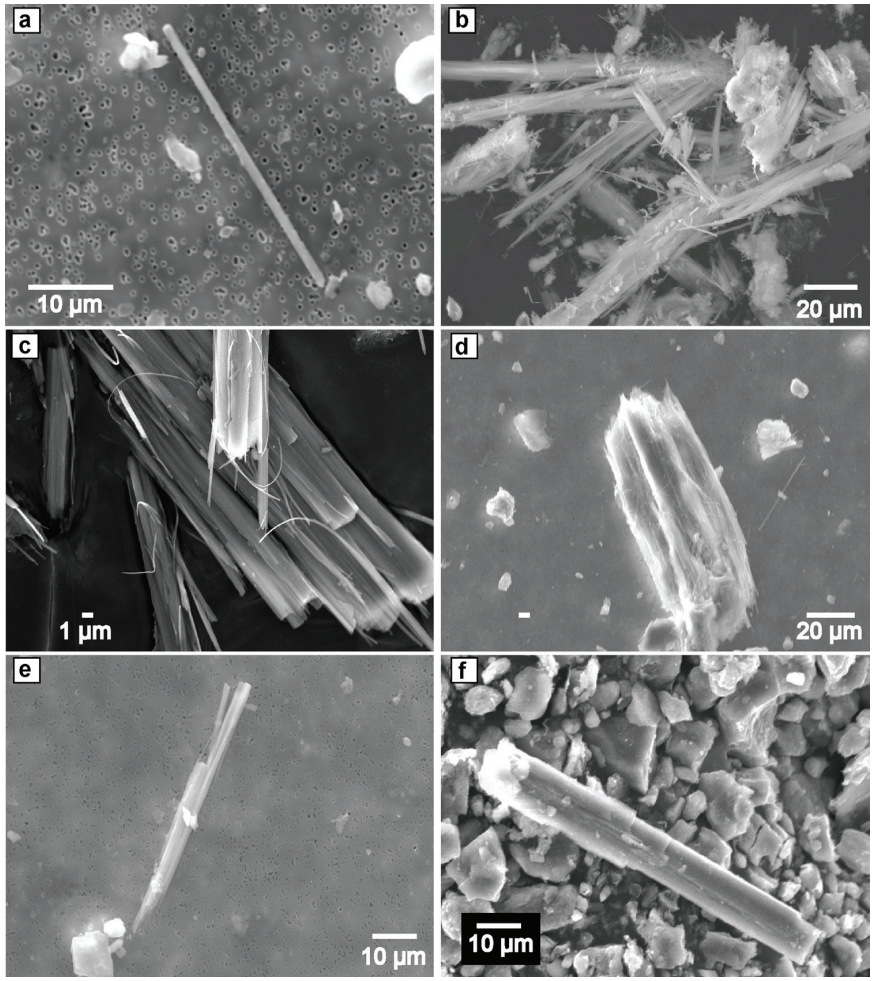

Fig. 4. Scanning electron microscope (SEM)/field-emission scanning electron microscope (FE-SEM) images: (a) amphibole fiber from soil in an alluvial fan along the western edge of Black Hill (Sample H7); (b) amphibole fiber bundles from rock at Martha P. King Elementary School (Sample Adams), Boulder City; (c) FE-SEM image of curling fibers from rock at Martha P. King Elementary School (Sample Adams); (d) amphibole fiber bundle from rock at Martha P. King Elementary School (Sample Adams 2); (e) amphibole fiber bundle from dust collected in dust trap in private yard in Boulder City (Sample D4); and (f) prismatic amphibole crystal from soil in an alluvial fan, near Highway 95 (Sample B9).

Length and width (diameter) were measured from 704 amphibole particles collected from rock, dust, and soils across the entire study area and from 61 amphibole particles collected from clothes and a car tire. Energy dispersive spectroscopy analysis was used to verify that these particles were amphibole (Fig. 6). An additional 259 visually identified fibrous particles were measured with FE-SEM, which did not have EDS capability. To distinguish between the identified and unidentified particles, we used color for the former and gray for the latter in Fig. 7. Confirmed amphibole fiber length ranged from 3.9 to 67.6 µm (average 27.9 µm); confirmed amphibole particle length ranged from 3.6 to 308.2 µm (average 18.1 µm). Confirmed amphibole average particle width was 3.9 µm (particles) and 1.2 µm (fibers). Sixty-nine percent of the amphibole particles measured and 97% of amphibole fibers were <3 µm in diameter and are thus considered respirable (National Research Council, 1984, p. 25–47). Fibers with aspect ratios >3:1 and those that are longer than 5 µm are more toxic (Aust et al., 2011; Case et al., 2011). In this study, we found that 100% of all amphibole fibers and 97% of all amphibole particles had aspect ratios >3:1 (Fig. 8).

To find out how these particles will be transported through air, the annual frequency distribution of the wind's friction velocity in the area was determined (Fig. 9a). The meteorological stations in Henderson and Boulder City do not record friction velocities, but during a previous project a detailed data set was collected from Nellis Dunes Recreational Area, which is located approximately 8 km northeast of Las Vegas and has similar terrain types (data are available on request). For the 765 EDS-confirmed fibrous amphibole particles investigated in this study, the four transport modes of saltation, modified saltation, short-term suspension, and long-term suspension were calculated using the friction velocity classes shown in Fig. 9a. The results show that even at very low friction velocities, almost all of the amphiboles will be transported in suspension (Fig. 9b).

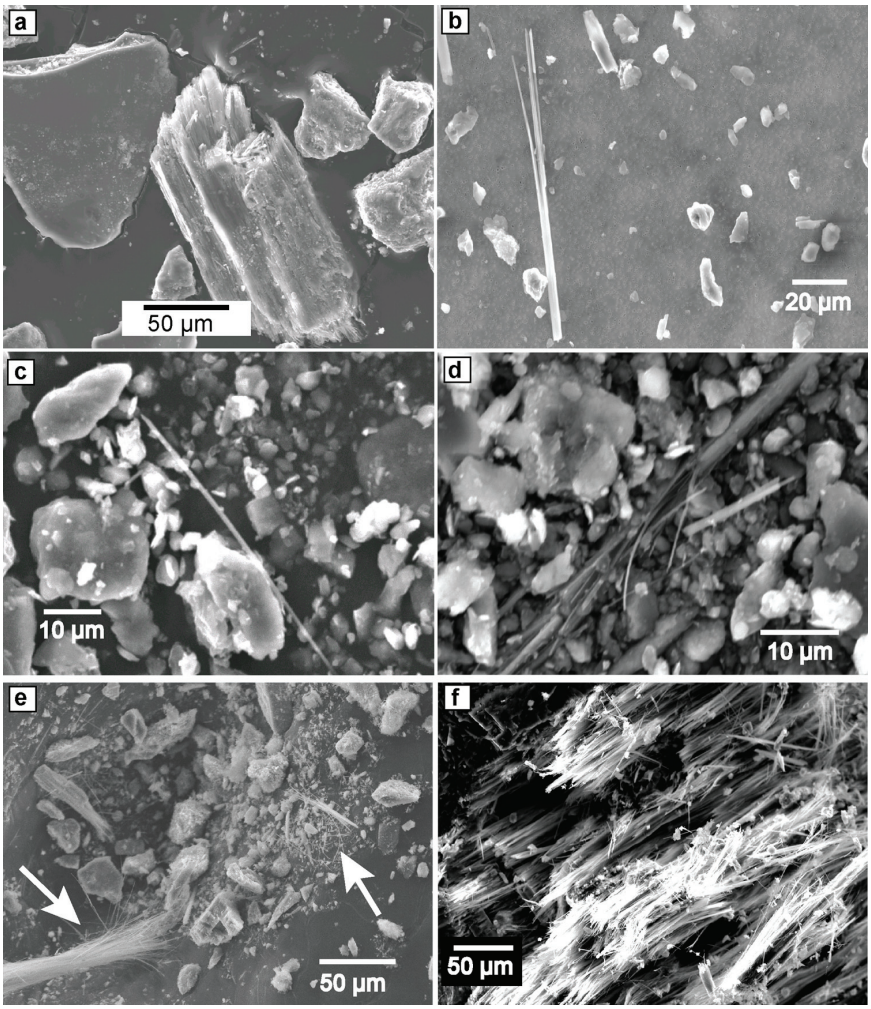

Fig. 5. Scanning electron microscope images: (a) amphibole crystal with frayed ends collected as dust generated from car driving on dirt road, Boulder City (Sample BCF); (b) amphibole bundle from soil in an alluvial fan, western side of Black Hill (Sample H5); (c) amphibole fiber from soil in an alluvial fan, near Highway 95 (Sample B10); (d) amphibole bundle from soil in an alluvial fan south of Boulder City (Sample B8); (e) asbestiform amphiboles from broken rock collected in McCullough Range (Sample RJ1); and (f) fibrous amphibole from rock in southern Boulder City (Sample BCP 1).

DISCUSSION

Although more particles need to be measured in future studies, our data suggest that the morphology of the fibers in southern Nevada is comparable to those in the Libby, MT, USEPA Superfund site (Meeker et al., 2003) and that the fibers are longer than those in El Dorado Hills, CA, a well-known area containing naturally occurring amphibole asbestos classified as actinolite and magnesiohornblende (Meeker et al., 2006) (Fig. 8). The average aspect ratio for our measured amphibole fibers was 16:1, which is less than the amphiboles measured at Libby, MT (Meeker et al., 2003), but much greater than those found in El Dorado Hills, CA (Meeker et al., 2006). Particles that are >5 µm in length and have aspect ratios >3:1 are countable as asbestos (Crane, 1995). Ninety-two percent of the fibers and 95% of all particles counted would meet this definition. As discussed in Meeker et al. (2003), some definitions of "true" asbestos require lengths >5 µm with aspect ratios >20:1. In this study, 28% of fibers met this definition. In general, the Nevada amphiboles have a significantly greater number of higher aspect ratio particles than the El Dorado Hills fibrous amphiboles (Meeker et al., 2006). In fact, their higher aspect ratio frequency is comparable to that of the Libby fibrous and asbestiform amphiboles (Meeker et al., 2003) and the anthophyllite and tremolite asbestos characterized by Campbell et al. (1977) (Fig. 8). Additionally, there is no sharp morphometric delineation between individual fibers, fiber bundles, and prismatic crystals but rather a very gradual transition (Fig. 7). The morphometry of the fibrous particles does not substantially change when the original bedrock weathers into soil; particles then become eroded, are transported through wind and/or water, and finally settle and accumulate on natural or other surfaces (Fig. 7). Although some granulometrical differentiation likely takes place during these processes, the data suggest that changes in shape remain small. Altogether, comparing their morphology with that in Libby, MT, and their identification as actinolite, one of the six regulated asbestos minerals, these data indicate that these fibers in southern Nevada are highly respirable and possibly carcinogenic.

The vast majority of the population of Clark County, 2 million in 2012 (U.S. Census Bureau 2013), is found in the conurbation of Las Vegas–Henderson–North Las Vegas (Fig. 1). Populations in Boulder City, Henderson, and probably the easternmost portions of Las Vegas may be exposed to these actinolite asbestos fibers. The most common exposure route would be through airborne dust. In this arid region, significant dust emissions are created through both (i) natural wind erosion (Fig. 10a) and (ii) any anthropogenic activities that disrupt the surface (Goossens et al., 2012) (Fig. 10b). Based on soil texture, vegetation, and visual evidence, the area most vulnerable to wind erosion is found south and southwest of Boulder City (Eldorado Dry Lake and the sandy surfaces east of Highway 95; see Fig. 2). Numerous types of anthropogenic activities occur or are planned throughout the area, and many dirt roads are present in the McCullough Range and surrounding Boulder City. In addition, the wind regime in the area is bimodal (Fig. 11), with strong south and southwest winds in spring and summer and primarily northeast winds in autumn and winter (Goossens and Buck, 2011). Southeast winds are less common but do occur. Therefore, especially in the spring, the populations of eastern Henderson and eastern Las Vegas are located within only a few hundred meters to a few kilometers downwind from the emission sources. In Boulder

City, the sources of amphibole fibers are even closer, with a potential for exposure year-round.

The aeolian transport mode can be used as a tool to estimate how far downwind the fibrous amphiboles can be transported once they are emitted and become airborne. Even at very low friction velocities, almost all of the measured amphibole particles will be transported in suspension (Fig. 9b). This means that, once airborne, they can easily reach the populated areas of Boulder City, eastern Henderson, and the eastern portions of Las Vegas, although for the latter, concentrations will be lower because of natural dilution. Especially for Boulder City, more research is needed because the populated zones are entirely situated within the source area of the fibrous amphiboles. Several outcrops of the pluton occur within the city itself, and the remaining part of the city has been built on soils derived from the pluton or on surfaces enriched with amphiboles transported by water and wind (Fig. 2). More outcrops of the pluton occur directly east and north of the city, and amphibole-enriched alluvial fans and sand surfaces prone to wind erosion are adjacent to the south. Therefore, populations in Boulder City are likely to be exposed to fibrous amphiboles regardless of wind direction, and anthropogenic activities can cause dust production year-round. No information is currently

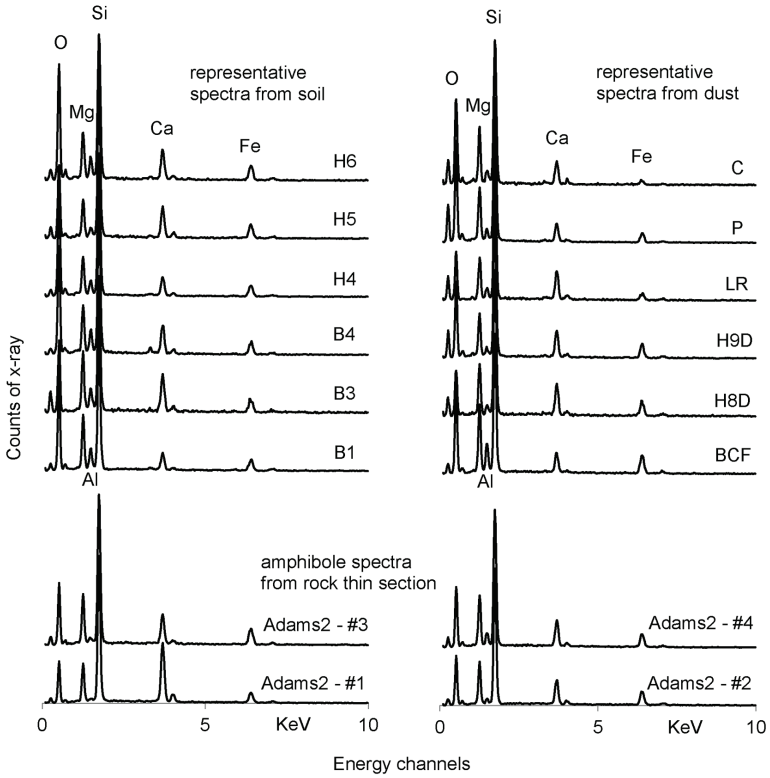

Fig. 6. Comparison of energy dispersive spectra of fibrous amphiboles representative of those collected from amphibole particles in soil (Samples H6 H5, H4, B4, B3, and B1) (upper left), collected from amphibole particles in dust (Samples H9D, H8D, and BCF), on clothes (Samples P and LR), or the car tire (Sample C) (upper right), and collected from polished thin sections of rocks collected from Boulder City (bottom). The spectra indicate similar amphibole compositions in dust (and clothes), soil, and rock.

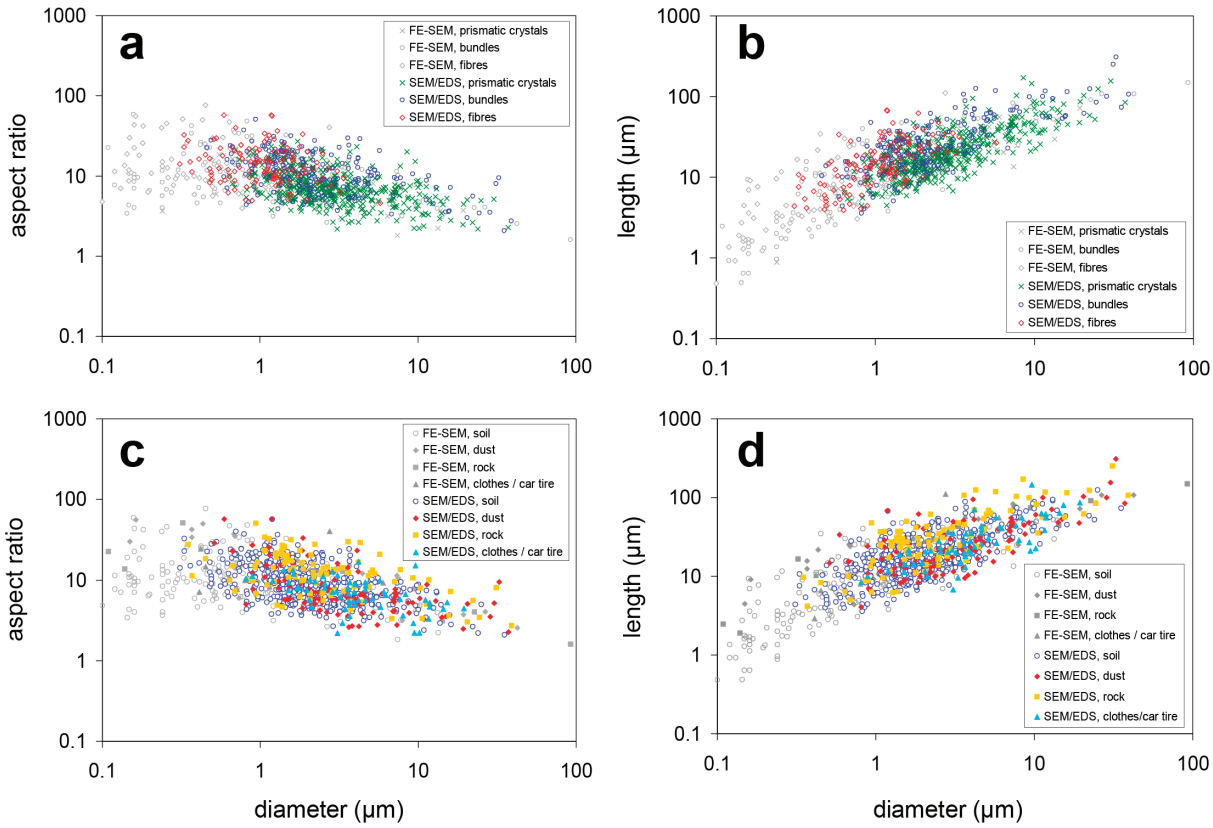

Fig. 7. Morphology of the Nevada fibrous amphiboles: (a) aspect ratio and (b) fiber length of all 1024 measured particles as a function of the particle diameter for the three morphological fiber types defined in this study, and (c) aspect ratio and (d) fiber length of the same 1024 particles as a function of the particle diameter for four different types of sources. Scanning electron microscope/energy dispersive spectroscopy (SEM/EDS)-confirmed amphiboles are shown in color; field-emission scanning electron microscope (FE-SEM) non-EDS-confirmed but visually identified amphiboles are shown in gray.

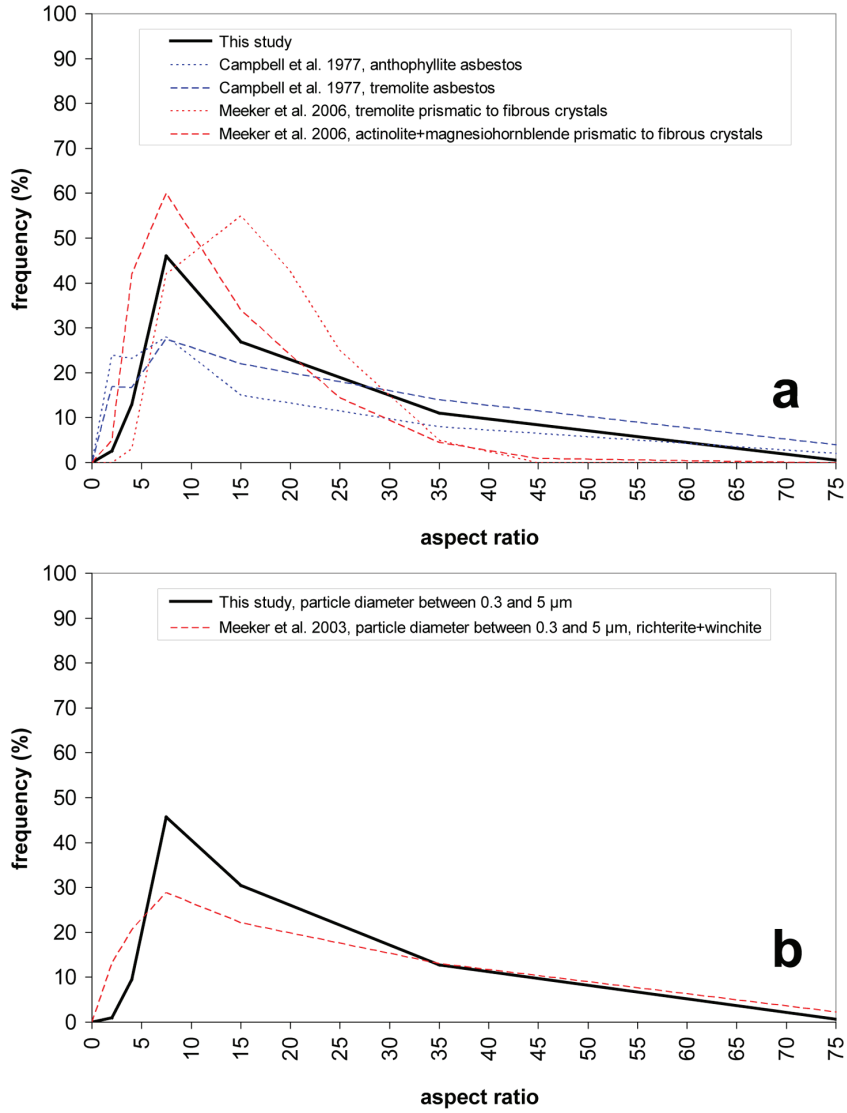

Fig. 8. Comparison with fibrous amphiboles from other sites: (a) energy dispersive spectroscopy (EDS)-confirmed amphiboles from this study vs. amphiboles (tremolite and actinolite + magnesiohornblende) from El Dorado Hills, CA (Meeker et al., 2006) and asbestos (anthophyllite and tremolite) analyzed in a U.S. Bureau of Mines study (Campbell et al. 1977); b. amphiboles from our study site vs. amphiboles (richterite and winchite) from Libby, MT (Meeker et al. 2003). The data for Libby, MT, are for particle diameters <5 μm and the minimum diameter for reliable EDS analysis in the Nevada study was 0.3 μm; therefore, the curves were calculated for the interval 0.3 to 5.0 μm, which represents 84% of the EDS-confirmed Nevada amphiboles. All curves are for total samples (individual fibers, fiber bundles, and/or prismatic crystals, in their original proportions).

available, however, on the actual airborne concentrations at any location in the county. This information is greatly needed to better understand potential health risks.

CONCLUSIONS

Given the mineralogy and morphology of these fibers, it is imperative that this problem be further studied in southern Nevada. In Libby, MT, exposure to fibrous amphiboles has resulted in asbestos-related-disease mortality rates 40 to 80 times higher than other areas in Montana and the United States (Agency for Toxic Substances and Disease Registry, 2002). In the arid climate of Nevada, populations may be exposed to these fibers through dust emissions that can occur from both natural wind erosion and anthropogenic activities. The evidence of fibrous amphiboles on car tires and on clothing after recreational activities shows that they can be brought back to family members and thus increase the risk of exposure for other populations besides those directly exposed through outdoor dust emissions. Because health effects may occur even at low levels of exposure to fibrous amphiboles (Alexander et al., 2011; Hillerdal, 1999), our data indicate a potential public health threat in southern Nevada. Any potential future land-use projects should carefully determine the risks to both workers and the regional populations because disturbances to these natural desert surfaces cause increased dust emissions (Goossens et al., 2012). Social behaviors and land management practices that limit dust production in areas where fibers are present could be implemented to reduce human exposure. There is a compelling need for epidemiology studies, additional geologic and mineral studies, and significantly more research on their location, emission, airborne concentration, and pathways of human exposure.

APPENDIX A

When terminal fall velocity is reached, flow resistance has become equal to the submerged particle weight:

$$G - F_B = F_W \qquad [1]$$

where G is the particle weight, F_B is the buoyancy force, and F_W is the flow resistance.

Since

$$G = \rho_p V g$$

$$F_B = \rho_f V g$$

and

$$F_W = \frac{C_D \rho_f u^2 A}{2}$$

where ρ_p is the particle's mass density, ρ_f is the fluid's mass density, V is the particle volume, g is gravitational acceleration, C_D is the drag coefficient, u is the particle velocity, and A is the particle's cross-sectional area perpendicular to the flow,

$$(\rho_p - \rho_f) V g = \frac{C_D \rho_f u^2 A}{2} \qquad [2]$$

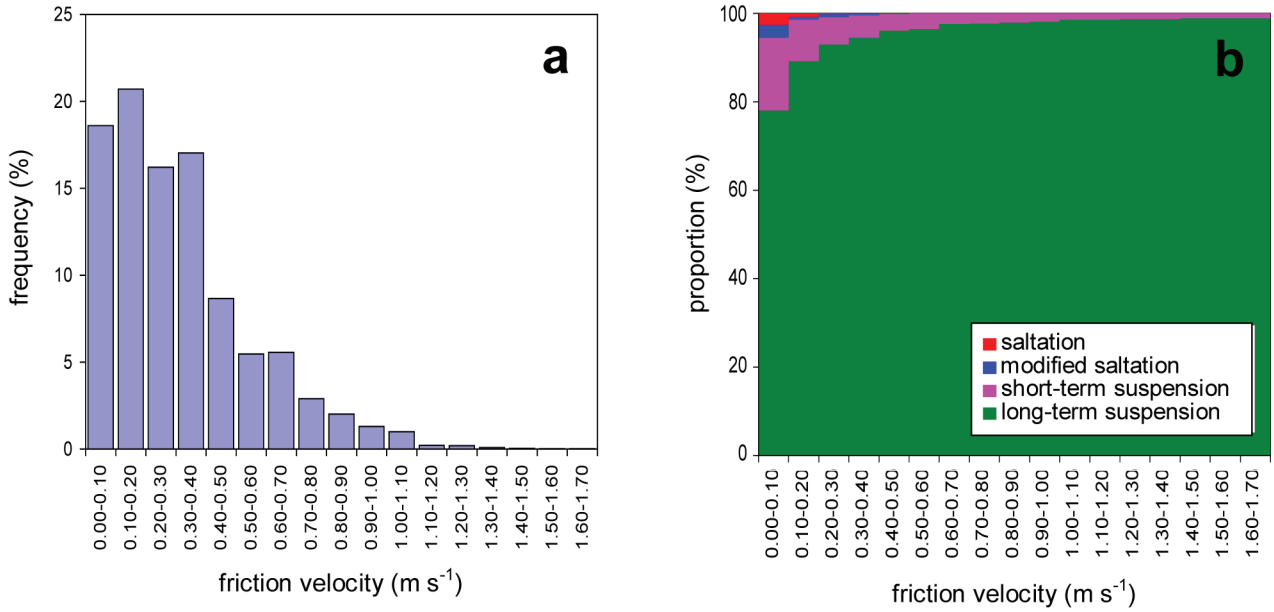

Fig. 9. Atmospheric transport modes: (a) annual frequency distribution of the wind's friction velocity near the study area; and (b) proportion of four aeolian transport modes calculated for the 765 energy dispersive spectroscopy (EDS)-confirmed fibrous amphibole particles measured in this study. Even at very low friction velocities, almost all of the amphiboles will be transported in suspension.

For a cylindrical particle of length L and radius R falling at an angle α (Fig. 12), the particle's volume is $LR^2\pi$ and the particle's cross-sectional area perpendicular to the flow is $R^2\pi\sin\alpha + 2RL\cos\alpha$. Therefore,

$$(\rho_p - \rho_f)LR^2\pi g = C_D \frac{\rho_f u^2}{2}(R^2\pi\sin\alpha + 2RL\cos\alpha) \qquad [3]$$

For a spherical particle in laminar flow (Re < 0.1), the drag coefficient is equal to 24/Re, where Re is the particle Reynolds number (Prandtl and Tietjens, 1934). For Re between 0.1 and 1.0, this formula still gives a very good approximation (see Giles, 1962). For nonspherical particles and Re <1.0, the drag coefficient can be written as (24/Re)S, where S is a dimensionless shape factor. A test with particles used in this study (Fig. 13) showed that for the range 0.001 < Re < 1 and $\alpha = 45°$ (see main text), very good results are obtained when S is set equal to unity. The following formula thus gives a very good approximation:

$$(\rho_p - \rho_f)LR^2\pi g = \frac{24}{\mathrm{Re}}\frac{\rho_f u^2}{2}(R^2\pi\sin\alpha + 2RL\cos\alpha) \qquad [4]$$

Rearranging Eq. [4]:

$$\left(\frac{\rho_p - \rho_f}{\rho_f}\right)LR\pi g = \frac{12}{\mathrm{Re}}u^2(R\pi\sin\alpha + 2L\cos\alpha) \qquad [5]$$

Writing Re as

$$Eu\frac{\rho_f}{\eta_f}$$

where E is the particle diameter and η_f is the fluid's dynamic viscosity:

$$\left(\frac{\rho_p - \rho_f}{\rho_f}\right)LR\pi g = \frac{12}{Eu}\frac{\eta_f}{\rho_f}u^2(R\pi\sin\alpha + 2L\cos\alpha) \qquad [6]$$

or

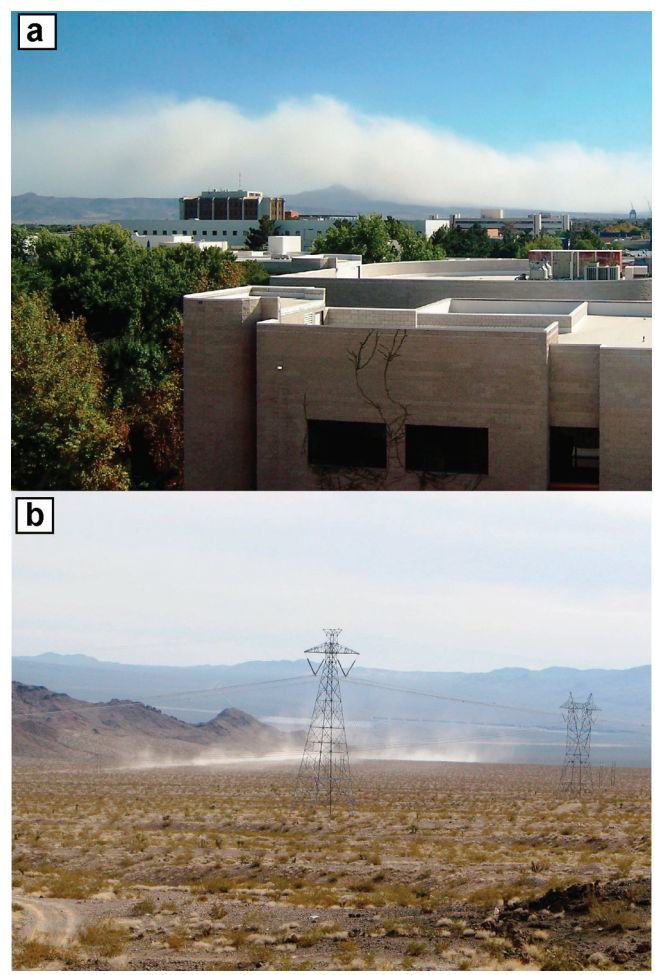

Fig. 10. Natural and anthropogenically produced dust: (a) a dust storm entering Henderson–Las Vegas from the south; the McCullough Range is obscured by dust; (b) dust generated by a single off-road vehicle driving on a dirt road in the McCullough Range.

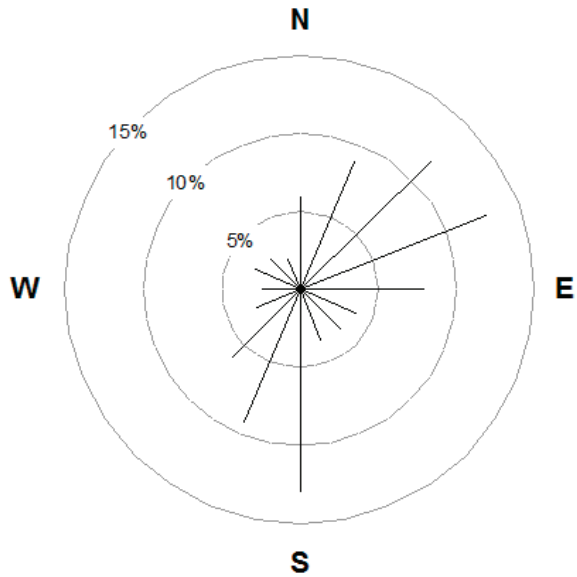

Fig. 11. Wind rose for the Las Vegas area. Percentages are based on hourly data and refer to the period 19 Dec. 2007 to 15 Dec. 2008 (data from Nellis Air Force Base meteorological station).

$$\left(\rho_p-\rho_f\right)LR\pi g=\frac{12}{E}\eta_f u\left(R\pi\sin\alpha+2L\cos\alpha\right) \qquad [7]$$

Hence,

$$u=\frac{\left(\rho_p-\rho_f\right)LR\pi gE}{12\eta_f\left(R\pi\sin\alpha+2L\cos\alpha\right)} \qquad [8]$$

Choosing the volume equivalent diameter D_{eq} to represent the particle's diameter in Re $\left(D_{eq}=\sqrt[3]{6LR^2}\right)$:

$$u=\frac{\left(\rho_p-\rho_f\right)LR\pi g\sqrt[3]{6LR^2}}{12\eta_f\left(R\pi\sin\alpha+2L\cos\alpha\right)} \qquad [9]$$

and after simplification:

$$u=\frac{\left(\rho_p-\rho_f\right)\pi g\sqrt[3]{6L^4R^5}}{12\eta_f\left(R\pi\sin\alpha+2L\cos\alpha\right)} \qquad [10]$$

ACKNOWLEDGMENTS

Thanks to R. Johnsen, G. Smith, O. Tschauner, P. Rees, S. Schafer, D. Merkler, and three anonymous reviewers. Funding provided by the University of Hawaii Cancer Center.

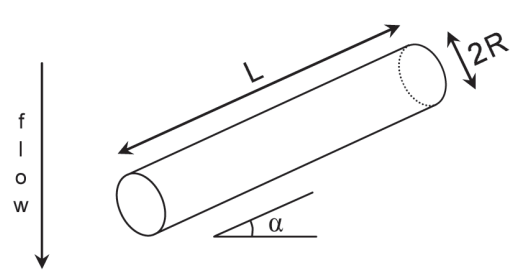

Fig. 12. Cylindrical particle of length *L* and radius *R* falling at an angle α.

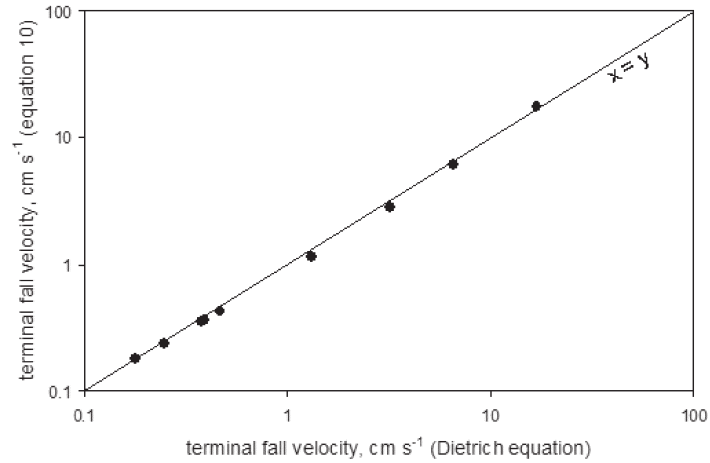

Fig. 13. Terminal fall velocities of particles in this study calculated with the equation of Dietrich (1982) and with Eq. [10]. The covered particle Reynolds number interval is $0.001 < R_e < 1$.

REFERENCES

Agency for Toxic Substances and Disease Registry. 2001. Toxicological profile for asbestos. ATSDR, Atlanta, GA. http://www.atsdr.cdc.gov/toxprofiles/tp61.pdf (accessed 17 Nov. 2012).

Agency for Toxic Substances and Disease Registry. 2002. Mortality in Libby, Montana (1979–1998). ATSDR, Atlanta, GA.

Alexander, B., K. Raleigh, J. Johnson, J. Mandel, J. Adgate, G. Ramachandran, et al. 2011. Radiographic evidence of nonoccupational asbestos exposure from processing Libby vermiculite in Minneapolis, Minnesota. Environ. Health Perspect. 120:44–49. doi:10.1289/ehp.1103529

Anderson, R.E. 1977. Geologic map of the Boulder City 15-minute quadrangle, Clark County, Nevada. USGS Map GQ-1395. USGS, Reston, VA.

Ahn, J.H., and P.R. Buseck. 1991. Microstructures and fiber-formation mechanisms of crocidolite asbestos. Am. Mineral. 76:1467–1478.

Aust, A., P. Cook, and R. Dodson. 2011. Morphological and chemical mechanisms of elongated particle toxicities. J. Toxicol. Environ. Health, Part B 14:40–75. doi:10.1080/10937404.2011.556046

Baumann, F., P. Maurizot, M. Mangeas, J. Ambrosi, J. Douwes, and B. Robineau. 2010. Pleural mesothelioma in New Caledonia: Associations with environmental risk factors. Environ. Health Perspect. 119:695–700. doi:10.1289/ehp.1002862

Camargo, M., L. Stayner, K. Straif, M. Reina, U. Al-Alem, P. Demers, and P. Landrigan. 2011. Occupational exposure to asbestos and ovarian cancer. Environ. Health Perspect. 119:1211–1217. doi:10.1289/ehp.1003283

Campbell, W., R. Blake, L. Brown, E. Cather, and J. Sjoberg. 1977. Selected silicate minerals and their asbestiform varieties: Mineralogical definitions and identification-characterization. Inf. Circ. 8751. U.S. Bureau of Mines, Washington, DC.

Carbone, M., Y. Baris, P. Bertino, B. Brass, S. Comertpay, A. Dogan, et al. 2011. Erionite exposure in North Dakota and Turkish villages with mesothelioma. Proc. Natl. Acad. Sci. 108:13618–13623. doi:10.1073/pnas.1105887108

Case, B., J. Abraham, G. Meeker, F. Pooley, and K. Pinkerton. 2011. Applying definitions of "asbestos" to environmental and "low-dose" exposure levels and health effects, particularly malignant mesothelioma. J. Toxicol. Environ. Health, Part B 14:3–39. doi:10.1080/10937404.2011.556045

Corey, A.T. 1949. Influence of shape on the fall velocity of sand grains. M.S. thesis. Colorado A&M College, Fort Collins.

Crane, D.T. 1995. Polarized light microscopy of asbestos. OSHA Method ID-191 (revised 1995). Occup. Saf. Health Admin., Washington, DC. http://www.osha.gov/dts/sltc/methods/inorganic/id191/id191.html (accessed 4 Apr. 2013).

Dietrich, W.E. 1982. Settling velocity of natural particles. Water Resour. Res. 18:1615–1626. doi:10.1029/WR018i006p01615

Felger, T.J., and L.S. Beard. 2010. Geologic map of Lake Mead and surrounding regions, southern Nevada, southwest Utah, and northwestern Arizona. In: P.J. Umhoefer et al., editors, Miocene tectonics of the Lake Mead region, Central Basin and Range. Spec. Pap. 463. Geol. Soc. Am., Boulder, CO. p. 29–38.

Folk, R.L. 1965. Student operator error in determination of roundness, sphericity and grain size. J. Sediment. Petrol. 25:297–301.

Fryrear, D. 1986. A field dust sampler. J. Soil Water Conserv. 41:117–120.

Giles, R.V. 1962. Fluid mechanics and hydraulics. 2nd ed. Schaum Publ. Co., New York.

Goossens, D. 1987a. A drag coefficient equation for natural, irregularly shaped particles. Catena 14:73–99. doi:10.1016/S0341-8162(87)80007-3

Goossens, D. 1987b. Sedimentatiemechanismen bij Natuurlijke Stofdeeltjes in Lucht. Ph.D. diss. Katholieke Univ. Leuven, Leuven, Belgium.

Goossens, D., and B. Buck. 2011. Effects of wind erosion, off-road vehicular activity, atmospheric conditions and the proximity of a metropolitan area on PM10 characteristics in a recreational site. Atmos. Environ. 45:94–107. doi:10.1016/j.atmosenv.2010.09.046

Goossens, D., B. Buck, and B. McLaurin. 2012. Contributions to atmospheric dust production of natural and anthropogenic emissions in a recreational area designated for off-road vehicular activity (Nellis Dunes, Nevada, USA). J. Arid Environ. 78:80–99. doi:10.1016/j.jaridenv.2011.10.015

Harper, M. 2008. 10th Anniversary critical review: Naturally occurring asbestos. J. Environ. Monit. 10:1394–1408. doi:10.1039/b810541n

Hawthorne, F., R. Oberti, G. Harlow, W. Maresch, R. Martin, J. Schumacher, and M. Welch. 2012. Nomenclature of the amphibole super group. Am. Mineral. 97:2031–2048. doi:10.2138/am.2012.4276

Hillerdal, G. 1999. Cases associated with non-occupational and low dose exposures. Occup. Environ. Med. 56:505–513. doi:10.1136/oem.56.8.505

House, P.K., H. Green, and A. Grimmer, and Nevada Digital Dirt Mapping Team. 2010. Preliminary surficial geologic map of Clark County, Nevada. Open-File Rep. 10-7. Nevada Bureau of Mines and Geology, Reno.

International Agency for Research on Cancer. 2012. Asbestos. In: A review of human carcinogens. IARC Monogr. Eval. Carcinogenic Risks to Humans 100C. WHO Press, Lyon, France. p. 219–294.

Leake, B.E. 1978. Nomenclature of amphiboles. Can. Mineral. 16:501–520.

Leake, B.E., A. Woolley, C. Arps, W. Birch, M. Gilbert, J. Grice, et al. 1997. Nomenclature of the amphiboles: Report of the subcommittee on amphiboles of the International Mineralogical Association, Commission on New Minerals and Mineral Names. Am. Mineral. 82:1019–1037.

Lowers, H., and G. Meeker. 2002. Tabulation of asbestos-related terminology. USGS Open-File Rep. 02-458. USGS, Reston, VA. http://pubs.usgs.gov/of/2002/ofr-02-458/index.html (accessed 18 Apr. 2013).

Meeker, G. 2009. Asbestos *sans* mineralogy? A view from a different hilltop. Elements 5:269.

Meeker, G., A. Bern, I. Brownfield, H. Lowers, S. Sutley, T. Hoefen, and J. Vance. 2003. The composition and morphology of amphiboles from the Rainy Creek Complex near Libby, Montana. Am. Mineral. 88:1955–1969.

Meeker, G., H. Lowers, G. Swayze, B. Van Gosen, S. Sutley, and I. Brownfield. 2006. Mineralogy and morphology of amphiboles observed in soils and rocks in El Dorado Hills, California. USGS Open-File Rep. 2006-1362. USGS, Reston, VA.

National Research Council. 1984. Asbestiform fibers: Nonoccupational health risks. Natl. Acad. Press, Washington, DC.

Potts, D.A. 2000. Sodium metasomatism and magnesio-riebeckite mineralization in the Wilson Ridge pluton. M.S. thesis. Univ. of Nevada, Las Vegas.

Potts, D.A., and R.V. Metcalf. 1997. Sodium metasomatism and riebeckite mineralization in an extensional terrane: Wilson Ridge pluton, northwest Arizona. Geol. Soc. Am. Abstr. 29(5):57.

Prandtl, L., and O.G. Tietjens. 1934. Applied hydro- and aeromechanics. Dover Publ., New York.

Pye, K., and H. Tsoar. 1990. Aeolian sand and sand dunes. Unwin Hyman, London.

Ryan, P., M. Dihle, S. Griffin, C. Partridge, T. Hilbert, R. Taylor, et al. 2011. Erionite in road gravel associated with interstitial and pleural changes: An occupational hazard in western United States. J. Occup. Environ. Med. 53:893–899.

Shannahan, J., M. Schladweiler, R. Thomas, W. Ward, A. Ghio, S. Gavett, and U. Kodavanti. 2012. Vascular and thrombogenic effects of pulmonary exposure to Libby amphibole. J. Toxicol. Environ. Health A 75:213–231. doi:10.1080/15287394.2012.652055

Smith, E.I. 1984. Geologic map of the Boulder Beach quadrangle, Nevada. Map 81. Nevada Bureau of Mines and Geology, Reno.

U.S. Census Bureau. 2013. State & county QuickFacts: Clark County, Nevada. U.S. Census Bureau, Washington, DC. http://quickfacts.census.gov/qfd/states/32/32003.html (accessed 18 Apr. 2013).

Vakil, A., and S.I. Green. 2009. Drag and lift coefficients of inclined finite circular cylinders at moderate Reynolds numbers. Comput. Fluids 38:1771–1781. doi:10.1016/j.compfluid.2009.03.006

Van Gosen, B. 2008. Reported historic asbestos mines, historic asbestos prospects, and natural asbestos occurrences in the southwestern United States (Arizona, Nevada, and Utah). USGS Open-File Rep. 2008-1095. USGS, Denver, CO.

Virta, R. 2002. Asbestos: Geology, mineralogy, mining, and uses. USGS Open-File Rep. 02-149. USGS, Reston, VA.

Williams, M.M. 2003. Depositional history of the Black Mountain conglomerate, Mohave County, Arizona: Sedimentary response to Miocene extension. M.S. thesis. Univ. of Nevada, Las Vegas.

Wozniak, H., E. Wiecek, and J. Stetkiewicz. 1988. Fibrogenic and carcinogenic effects of antigorite. Pol. J. Occup. Med. Environ. Health 1:192–202.